Highly Selective Population of Spin-Orbit Levels in Electronic Autoionization of O_2

Paul-Marie Guyon and John W. Hepburn[a]
Laboratoire des Collisions Atomiques et Moléculaires, Université Paris XI, Bâtiment 351, 91405 Orsay, France

Taimeng Weng
Laboratoire pour l'Utilisation du Rayonnement Electromagnétique, Université Paris XI, Bâtiment 209D, 91405 Orsay, France

Franz Heiser
Fritz Haber Institut der Max Plank Gesellshaft, Faradayweg, 1000 Berlin, Germany

David Reynolds
Department of Chemistry, University of Nottingham, Nottingham, United Kingdom
(Received 25 March 1991)

The dynamics of electronic autoionization in O_2 has been studied using a new apparatus which combines a free-jet supersonic expansion with synchrotron radiation. Ions and electrons were analyzed by a double time-of-flight spectrometer. The spin-orbit sublevels of the $H\,^3\Pi_u$ ($v=0$ and 2) Rydberg states in O_2 were selectively excited and the resulting O_2^+ final states were determined by time-of-flight photoelectron spectroscopy. A strong variation of the $^2\Pi_{1/2g}$:$^2\Pi_{3/2g}$ branching ratio was observed. This variation results from the selection of a single continuum wave function in the autoionization process.

PACS numbers: 33.20.Ni, 33.60.Cv, 33.80.Eh

Photoionization of molecular oxygen near the ionization threshold shows intense autoionization peaks superimposed on a weak continuum. Some of these resonances, assigned to Rydberg series converging to O_2^+ $a\,^4\Pi_u$, were seen to be split into several components in the high-resolution photoionization spectrum of Dehmer and Chupka [1]. Recently, Tonkyn, Winniczek, and White observed a small portion of the spectrum comprising the $H\,^3\Pi_u \leftarrow {}^3\Sigma_g^-$ (2,0), (1,0), and (0,0) bands at still higher resolution using a vacuum-ultraviolet (VUV) laser for excitation of a supersonically cooled beam of oxygen molecules [2,3]. These authors also interpreted the fine structure and determined the spin-orbit constant from a fit of their photoionization spectrum using a pure $^3\Pi_u \leftarrow {}^3\Sigma_g^-$ transition within the Hund's case a coupling scheme. These series autoionize to the O_2^+ ground state and the observed vibrational branching ratio is consistent with the model of Bardsley and Smith for electronic autoionization [4–7]. The most recent photoelectron spectroscopic studies of this system by Holland and West [8] and by Tonkyn, Winniczek, and White [3] did not resolve the two $\Omega^+ = \frac{1}{2}$ and $\Omega^+ = \frac{3}{2}$ spin-orbit components of the $^2\Pi_g$ ground-state vibrational levels.

For these reasons, the investigation of the variation of the $^2\Pi_{1/2g}$:$^2\Pi_{3/2g}$ branching ratio upon selective excitation of the F_1, F_2, and F_3 spin-orbit components of the $H(v=0)$ and $H(v=2)$ excited states was undertaken. Experiments were carried out using a 3-m normal-incidence monochromator installed on SuperACO, the new synchrotron radiation source in Orsay, and a free-expansion jet adapted to a double electron-ion time-of-flight coincidence analyzer [9]. This apparatus made it possible to resolve low-energy photoelectron peaks separated by about 5 meV at energies as low as 10 meV, allowing us to resolve the spin-orbit components of the O_2^+ $^2\Pi_g$ state. The results presented here show a strong variation of this branching ratio across the $^3\Pi_u$ resonance profiles which is interpreted as due to a selection rule in the choice of the ionization continuum to which the resonances are coupled.

The details of the experimental setup will be given in a forthcoming paper and only the essential features will be outlined here. Photoelectrons and ions were extracted in opposite directions at right angles to both the jet and the photon beam. Photoelectrons were selected by both their time of flight (TOF), measured with respect to the photon pulse arrival time, and by angular discrimination [10]. The threshold electrons reached the detector in about 100 ns, less than the 120-ns photon pulse period when the ring was operated in the two-bunch mode. Energetic electrons arrived sooner or later depending on whether they were emitted forward or backward with respect to the detector direction. In the present experiment, the TOF analyzer was mounted perpendicular to the orbit of the synchrotron ring, at 90° from the VUV polarization vector.

The monochromator was operated at a bandwidth of 0.02 nm, i.e., 2.5 meV around 102.65 nm, the ionization threshold of O_2. The target beam was formed by expanding pure oxygen gas from a 20-μm pin hole, with the nozzle about 1 cm from the VUV beam. The actual temperature of the jet could not be determined.

The photoionization efficiency curve of the O_2 $H\,^3\Pi_u(v=0)$ Rydberg state is shown in Fig. 1. This spectrum closely resembles that obtained by Tonkyn, Winniczek, and White [3] using a pure beam of oxygen so that the peak maxima may be assigned to the rotational bandheads of the three spin-orbit components. We chose these maxima, namely, $\lambda = 100.38$, 100.31, and 100.26 nm for $H(v=0)$ and $\lambda = 98.31$, 98.26, and 98.20

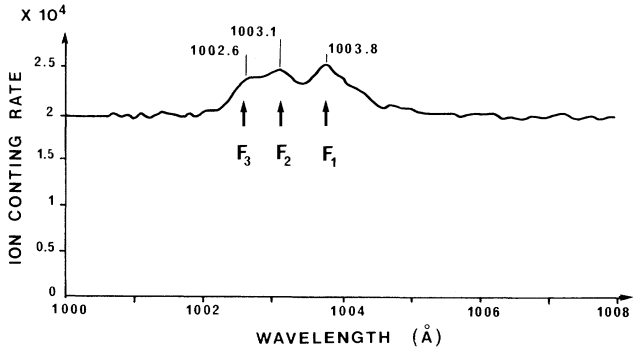

FIG. 1. Photoionization efficiency curve of O_2 in the region of the $H \leftarrow X(0,0)$ band. Underlying continuum signal is largely due to second-order light.

nm for $H(v=2)$, respectively, to excite selectively the F_i $(i=1,2,3)$ sublevels. The $H(v=0)$ and $H(v=2)$ peaks were superimposed upon a continuum due to direct ionization and ionization by light at the second-order wavelength. The latter, which results primarily in fast electrons, did not affect the present TOF spectra significantly.

The electron time-of-flight spectra obtained upon excitation of the $H(v=0)$ and $H(v=2)$ F_1, F_2, and F_3 components are shown in Figs. 2 and 3, respectively. They were roughly symmetrical with respect to the time of flight of the zero-energy electrons because of the contribution of both the forward and backward ejected electrons produced in the excitation region. One observes that the lowest-energy peaks are split into their two spin-orbit components $\Omega^+ = \frac{1}{2}$ and $\frac{3}{2}$. They are associated with O_2^+ $v=1$ and 2, respectively. The variation in the $^2\Pi_{1/2g}$:$^2\Pi_{3/2g}$ branching ratio with excitation energy is dramatic and clearly indicates a strong correlation between Ω and Ω^+, the projections of the total angular momentum on the molecular axis.

To interpret the TOF intensities, a direct measurement of the transmission function of the electron analyzer was performed by exciting Ar gas at the $^2P_{1/2}$ threshold and above. Over the energy range of interest, the transmission function was given by the electron signal as a function of electron energy, since the asymmetry parameter β is known to be constant and close to 0, and the ionization cross section is essentially wavelength independent [11]. The resulting transmission function is shown in Fig. 4. The intensity of the O_2^+ Ω^+ lines was then obtained by dividing the peak areas from the time-of-flight spectrum by the transmission at the electron energy corresponding to the peak maxima. The slight variation of the electron angular distribution over the resonance profile as measured by Tonkyn, Winniczek, and White [3] does not significantly affect the relative peak intensities and was neglected.

A second method used to analyze the time-of-flight spectra was a Monte Carlo simulation, the details of which will be published later. The coefficients for the two

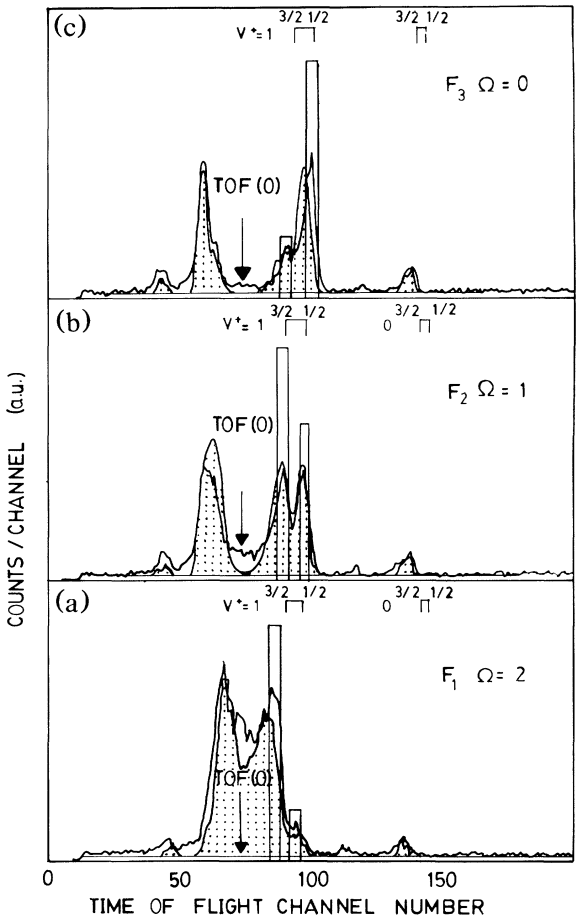

FIG. 2. TOF photoelectron spectra of O_2 obtained upon excitation of the $H \leftarrow X(0,0)$ band at (a) $\lambda = 100.38$ nm, (b) $\lambda = 100.31$ nm, and (c) $\lambda = 100.26$ nm. Histogram bars represent the peak area divided by transmission at the corresponding photoelectron energy (see Table I for values). Smooth curves shaded by dots are the result of the simulation described in the text. TOF(0) indicates the time of flight for zero-energy electrons.

Ω^+ components of each vibrational transition were adjusted for the best fit with the experimental spectrum; the results of such fits for the $H(v=0)$ state are shown in Fig. 2. The branching ratios obtained by both methods are given in Table I. Because of the poorer resolution and statistics, the fine structure of the highest-energy photoelectron peaks was not analyzed, but one can see from the spectra that the branching ratios observed for the lowest-energy photoelectron peaks are consistent with the shapes of the higher-energy peaks.

The good agreement between the two analyses of the spectra shows with no ambiguity the following correlations:

$$F_1 \rightarrow {}^2\Pi_{3/2}, \quad F_2 \rightarrow {}^2\Pi_{1/2} + {}^2\Pi_{3/2}, \quad F_3 \rightarrow {}^2\Pi_{1/2}. \qquad (1)$$

It should be stressed that the present measurement gives only a lower limit for the selectivity for two reasons. First, pure F_i states were not excited because of the finite

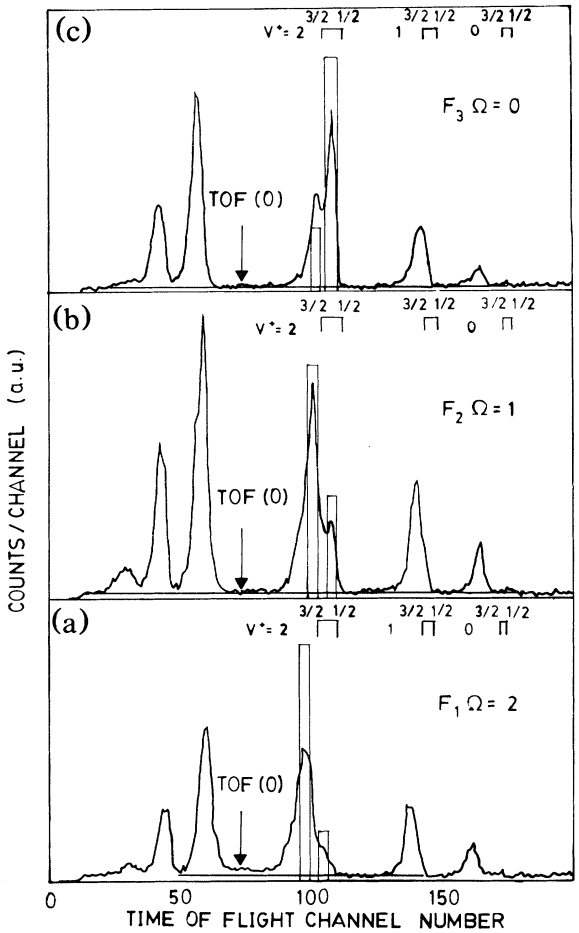

FIG. 3. TOF photoelectron spectra of O_2 obtained upon excitation of the $H \leftarrow X(2,0)$ band at (a) $\lambda = 98.31$ nm, (b) $\lambda = 98.26$ nm, and (c) $\lambda = 98.195$ nm. Bars indicate peak area divided by transmission.

width of the rotational envelope. Second, there is a contribution to the signal, albeit small, from the direct ionization process, which will populate both states with the same probability.

The assignment of the $H\,^3\Pi_u$ lines to a Rydberg series converging to the $a\,^4\Pi_u$ state of the ion proposed by Nishitani *et al.* [12] can easily be obtained from consideration of the effective principal quantum number n^* which is found equal to 1.94 for $H(v=0)$, thus yielding $n=3$ and a quantum defect $\delta = 1.06$ which corresponds for first-row elements to a $3s$ Rydberg orbital. The $H(0)$ state thus has a $(\pi_u)^3(\pi_g)^2(3s\sigma_g)$ configuration. Being the lowest member of the Rydberg series and having a large spin-orbit coupling, it is appropriate to describe it within the Hund's case a coupling scheme $\Lambda = 1$, $\Omega = 0,1,2$. Tonkyn, Winniczek, and White [3] have estimated the spin-orbit constant from a fit of the photoionization spectrum using the known value $A = -47.8$ cm^{-1} for the $a\,^4\Pi_u$ state as the initial guess. Their value $A = -60$ cm^{-1} is confirmed by calculation [13]. Since the simulation would not fit the spectrum if the sign of A were incorrect, the evidence for a negative A is strong. However, they erroneously assigned the value $\Omega = 0$ to F_1, the lowest-energy component of the triplet, and $\Omega = 2$ to F_3 which is inconsistent with a negative A value for an inverted state. The assignment we have used in our selective excitation is the correct one for negative A (F_1 is $\Omega = 2$, F_2 is $\Omega = 1$, and F_3 is $\Omega = 0$). A negative value for A for $a\,^4\Pi_u$ is consistent with the presence of an electron hole, i.e., $(\pi_u)^3$ or $(\pi_u)^{-1}$ configuration, as $A = 200$ cm^{-1} is positive for the ground-state ion with (π_g) configuration.

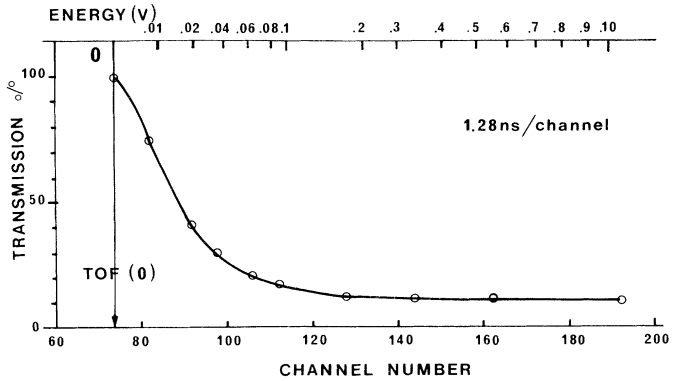

FIG. 4. Transmission function for electron time-of-flight spectrometer.

According to Kronig's selection rules the nonradiative homogeneous transitions are the following:

$$\Delta\Lambda = 0, \quad \Delta\Sigma = 0, \quad \Delta\Omega = 0, \quad \Delta J = 0. \tag{2}$$

The continuum states must be $^3\Pi_u$ for a pure Coulomb interaction, so that the two accessible continuum wave functions are σ_u or δ_u. The possible states that one can construct for $(\pi_g)(\sigma_u)$ and $(\pi_g)(\delta_u)$ configurations are shown in Table II.

We see that the conservation rules lead to opposite conclusions concerning the final spin-orbit component Ω^+ which is populated by autoionization of a given sublevel F_i of the $^3\Pi$ state according to the σ_u or the δ_u character of the continuum electron wave function.

The correlation between Ω and Ω^+ observed experimentally [expression (1)] and the negative A for the $H\,^3\Pi_u$ state signify that among two continua accessible according to selection rules for electronic autoionization the $H\,^3\Pi_u$ Rydberg series of the oxygen molecule decay almost entirely into σ_u. This in turn means that the bielectronic integrals of the type $\langle \pi_u \sigma_g | 1/r_{12} | \pi_g k\sigma_u \rangle$ are

TABLE I. $^2\Pi_{1/2}$:$^2\Pi_{3/2}$ branching ratio. In each entry, the first number given is the result of dividing the peak area by the transmission, and the second number was determined by Monte Carlo simulation.

Transition	F_1 ($\Omega = 2$)	F_2 ($\Omega = 1$)	F_3 ($\Omega = 0$)
$H(0) \rightarrow v^+ = 1$	0.22; 0.3	1.35; 1.43	4.3; 5
$H(2) \rightarrow v^+ = 3$	0.19; 0.24	0.47; 0.45	2.7; 2.5

TABLE II. Correlations between Rydberg and ion states.

Configuration	State	$\langle\Omega,\Sigma\vert = \langle\lambda^+,\sigma^+\vert\langle\lambda_c,\sigma_c\vert$	Ion state
$(\pi_g)(\sigma_u)$	$^3\Pi_2$	$\langle 2,1\vert = \langle 1,\frac{1}{2}\vert\langle 0,\frac{1}{2}\vert$ $\langle -2,-1\vert = \langle -1,-\frac{1}{2}\vert\langle 0,-\frac{1}{2}\vert$	$^2\Pi_{3/2}$
	$^3\Pi_1$	$\langle 1,0\vert = (1/\sqrt{2})\{\langle 1,\frac{1}{2}\vert\langle 0,-\frac{1}{2}\vert + \langle 1,-\frac{1}{2}\vert\langle 0,\frac{1}{2}\vert\}$ $\langle -1,0\vert = (1/\sqrt{2})\{\langle -1,-\frac{1}{2}\vert\langle 0,\frac{1}{2}\vert + \langle -1,\frac{1}{2}\vert\langle 0,-\frac{1}{2}\vert\}$	$^2\Pi_{3/2} + {}^2\Pi_{1/2}$
	$^3\Pi_0$	$\langle 0,1\vert = \langle -1,\frac{1}{2}\vert\langle 0,\frac{1}{2}\vert$ $\langle 0,-1\vert = \langle 1,-\frac{1}{2}\vert\langle 0,-\frac{1}{2}\vert$	$^2\Pi_{1/2}$
$(\pi_g)(\delta_u)$	$^3\Pi_2$	$\langle 2,1\vert = \langle -1,\frac{1}{2}\vert\langle 2,\frac{1}{2}\vert$ $\langle -2,-1\vert = \langle 1,-\frac{1}{2}\vert\langle -2,-\frac{1}{2}\vert$	$^2\Pi_{1/2}$
	$^3\Pi_1$	$\langle -1,0\vert = (1/\sqrt{2})\{\langle 1,-\frac{1}{2}\vert\langle -2,\frac{1}{2}\vert + \langle 1,\frac{1}{2}\vert\langle -2,-\frac{1}{2}\vert\}$ $\langle 1,0\vert = (1/\sqrt{2})\{\langle -1,-\frac{1}{2}\vert\langle 2,\frac{1}{2}\vert + \langle -1,\frac{1}{2}\vert\langle 2,-\frac{1}{2}\vert\}$	$^2\Pi_{3/2} + {}^2\Pi_{1/2}$
	$^3\Pi_0$	$\langle 0,1\vert = \langle 1,\frac{1}{2}\vert\langle -2,\frac{1}{2}\vert$ $\langle 0,-1\vert = \langle -1,-\frac{1}{2}\vert\langle 2,-\frac{1}{2}\vert$	$^2\Pi_{3/2}$

much greater than $\langle\pi_u\sigma_g\vert 1/r_{12}\vert\pi_g k\delta_u\rangle$. Two cautionary notes should be added at this point. Since the analyzer used had a strong angular discrimination, the selectivity observed could have been affected by this (i.e., if the σ_u continuum was favored at 90°, and the δ_u at 0°). There is no evidence for such an effect, so it was not considered here. As well, although the F_i assignments are certain for the $H(v=0)$ state, strong perturbations in the $H(v=2)$ state make them slightly less sure [3]. This could be why the selectivity observed was less strong in $H(v=2)$, but the overall effect still persists for this state, as should the F_i assignments.

The present work illustrates how high-resolution time-of-flight photoelectron spectroscopy combined with the continuous wavelength tuning provided by new synchrotron radiation sources can bring new information on the coupling of autoionized resonances with the ionization continuum. In the case of O_2 the experiment revealed a strong selection rule for the decay of the $H\,^3\Pi_u$ Rydberg series into the $^2\Pi_g$ ionization continuum which is illustrated by the variation of the $\Omega^+(\frac{1}{2}:\frac{3}{2})$ branching ratio by more than an order of magnitude along the line profiles. The method outlined here can be applied to other molecular systems provided that the combination of jet-cooled molecules with high-resolution photon source allows selective excitation of isolated resonances. It will be of interest in future work to study the $\Omega^+(\frac{1}{2}:\frac{3}{2})$ branching ratio for higher members of the series when the coupling scheme appropriate to describe the Rydberg states will gradually move from *a* to *e* [14], and for higher vibrational members of the same series because the coupling with dissociation continua, which is expected to vary strongly with *v*, may alter the pure $^3\Pi_u$ character of the resonance.

We are particularly thankful to P. Archirel for his help in the description of the quantum states, and to H. Lefebvre-Brion for her calculation of the spin-orbit constant. The help of the technical staff at Laboratoire pour l'Utilisation du Rayonnement Electromagnétique is also acknowledged. J.W.H. acknowledges the support of the Natural Sciences and Engineering Research Council, through the International Exchange Programme, and the Alfred P. Sloan Foundation; NATO is thanked for a grant (No. 04 0784 86).

[a]Permanent address: Department of Chemistry, University of Waterloo, Waterloo, Ontario, Canada N2L 3G1.

[1] P. M. Dehmer and W. A. Chupka, J. Chem. Phys. **62**, 4525 (1975).
[2] R. G. Tonkyn, J. W. Winniczek, and M. G. White, Chem. Phys. Lett. **164**, 137 (1989).
[3] R. G. Tonkyn, J. W. Winniczek, and M. G. White, J. Chem. Phys. **91**, 6632 (1989).
[4] K. Tanaka and I. Tanaka, J. Chem. Phys. **59**, 5042 (1973).
[5] J. H. Eland, J. Chem. Phys. **72**, 6015 (1980).
[6] L. F. A. Ferreira, thése d'état, Université Paris XI, Orsay, 1984 (unpublished); P. M. Guyon and L. F. A. Ferreira, in *Proceedings of the Workshop on Autoionization of Molecules* (ANL Report No. ANL-PHY-85-3, 1985), p. 129.
[7] A. L. Smith, Philos. Trans. Roy. Soc. London A **268**, 169 (1970).
[8] D. M. P. Holland and J. B. West, Z. Phys. D **4**, 367 (1987).
[9] M. R. Viard, O. Atabek, O. Dutuit, and P. M. Guyon, J. Chem. Phys. (to be published); M. R. Viard, thése d'etat, Université Paris XI, Orsay, 1987 (unpublished).
[10] T. Bear, P. M. Guyon, I. Nenner, A. Tabouche-Fouhaille, R. Botter, L. F. A. Ferreira, and T. R. Govers, J. Chem. Phys. **70**, 1585 (1979).
[11] D. M. P. Holland, J. L. Dehmer, and J. B. West, Nucl. Instrum. Methods **195**, 331 (1982).
[12] E. Nishitani, I. Tanaka, T. Kato, and I. Koyano, J. Chem. Phys. **81**, 3429 (1984).
[13] H. Lefebvre-Brion (private communication).
[14] H. Frolich, M. Glass-Maujean, and P. M. Guyon, J. Chem. Phys. **94**, 1102 (1991).